

Low-Rank Tensor Completion via Tensor Ring with Balanced Unfolding

Huyan Huang, Yipeng Liu, *Senior Member, IEEE*, Ce Zhu, *Fellow, IEEE*

Abstract—Tensor completion aims to recover a multi-dimensional array from its incomplete observations. Among the existing tensor decompositions, tensor ring (TR) is special for its cyclic structure. Due to this cycle, TR unfoldings may capture more global correlations than those of other decompositions in some applications. In this paper, we propose a novel low rank tensor completion based on TR with balanced unfolding, which generalizes the characteristic of balance in matrix completion. We first develop a sampling theorem for low rank TR completion, which suggests a class of balanced TR unfoldings. Using these balanced unfoldings, a new optimization model for tensor completion can be formed. The alternating direction method of multipliers (ADMM) is used to solve this optimization problem, which is called TRBU. Both the computational complexity and convergence are analyzed to show its performance improvement. The experiments on synthetic data verify the correctness of theoretic analysis, and the numerical results of real-world data demonstrate that the proposed method outperforms the state-of-the-art ones in terms of recovery accuracy.

Index Terms—low rank tensor completion, tensor ring decomposition, sampling theorem, balanced unfolding, alternating direction method of multipliers

I. INTRODUCTION

A tensor can be regarded as a multi-dimensional array whose entries are indexed by several continuous or discrete variables. Tensor is a natural way to represent the high-dimensional data, thus it preserves more intrinsic information than matrix when dealing with high-order data [1]–[3].

In practice, parts of the tensor entries are missing during data acquisition and transformation, tensor completion estimates the missing entries based on the assumption that most elements are correlated [4]. This correlation can be modeled as low-rank data structures which can be used in a series of applications, including signal processing [2], machine learning [5], remote sensing [6], computer vision [7], etc.

There are two main frameworks for tensor completion, namely, energy minimization as well as tensor rank minimization [8], [9], where the energy is usually a recovery error in the context of tensor completion and the definition of rank varies with diverse tensor decompositions. The first method is realized by means of the alternating least square (ALS), in which each core tensor is updated one by one while keeping

This research is supported by National Natural Science Foundation of China (NSFC, No. 61602091, No. 61571102). The corresponding author is Yipeng Liu.

All the authors are with School of Information and Communication Engineering, University of Electronic Science and Technology of China (UESTC), Chengdu, 611731, China. (email: huyanhuang@gmail.com, yipengliu@uestc.edu.cn).

others fixed [8]. The ALS-based method requires a pre-defined tensor rank, while the rank minimization does not.

Common forms of tensor decompositions are summarized as follows. The CANDECOMP/PARAFAC (CP) decomposition factorizes a d -order tensor $\mathcal{X} \in \mathbb{R}^{n \times \dots \times n}$ into a linear combination of rank-one tensors [1], thus the storage requirement of CP decomposition is $dnr + d$, where r is the CP rank [2]. However, the determination of CP rank is an NP-hard problem [10], and low CP rank approximation may involve numerical problems [2]. Therefore, low CP rank tensor completion usually recovers the missing data by iteratively updating its factors with a pre-defined CP rank [11]–[19]. Tucker decomposition decomposes a tensor into a set of matrices and one core tensor, which models a potential pattern of mutual interaction between components in different modes [1]. Low Tucker rank tensor completion minimizes the Tucker rank which is a vector and its entries are the ranks of the factor matrices, or optimizes factors on Tucker manifold with a fixed Tucker rank [4], [6], [7], [20]–[26]. However, the storage complexity of Tucker decomposition is $r^d + dnr$ for a d -order tensor, provided that $[r, \dots, r]^T$ is the Tucker rank, which still grows exponentially with respect to its dimension. Tensor singular value decomposition (t-SVD) factorizes a 3-way tensor into two orthogonal tensors and a f-diagonal tensor [27], and the tubal rank is defined as the number of non-vanishing singular tubes in the f-diagonal tensor. The minimization of tubal rank is often used for tensor completion [28]–[30]. The storage in low tubal rank representation is $2n^2r + nr^2$, where r is the tubal rank of a 3-order tensor. However, t-SVD can only deal with the 3-order data from a strict viewpoint, which seriously limits its application. In tensor train (TT) decomposition, a higher-order tensor is decomposed into a set of 3-order core tensors with two border factor matrices [31]. Tensor train is also called matrix product states (MPS) with open boundary conditions (OBC) in physics [2], [3]. The number of parameters in TT decomposition is $(d-2)nr^2 + 2nr$, suppose that $[r, \dots, r]^T$ is the TT rank. Completion through two frameworks can be found in [32]–[35]. TT decomposition has some problems, i.e., the intermediate ranks could be much larger than the side ones and this decomposition highly depends on permutation of tensor's dimension, which makes it hard to find the optimal representation. These shortcomings limit its practical applications [36]. The hierarchical Tucker (HT) decomposition factorizes a tensor like a tree with each degree of nodes less than or equal to 3 [1]. Its storage requirement is $dnr + (d-2)r^3 + r^2$, where $[r, \dots, r]^T$ is HT rank. A HT rank minimization model for tensor completion can be found in [37].

The recently proposed tensor ring (TR) decomposition represents a high-order tensor as a sequence of cyclically contracted 3-order tensors, which has a periodic boundary conditions (PBC) [38], [39]. The main difference is that TR contains cycle while no cycle is included in TT. The cycle forces TR rank to be balanced and TR rank is consistently invariant under the cyclic permutation of the factors. The storage complexity is dnr^2 , where $[r, \dots, r]^T$ is the TR rank. However, the current ALS-based method (TR-ALS) is time-consuming [36], which can not process large-scale data efficiently. Furthermore, the overfitting problem occurs in TR completion with a small number of observations when TR rank is large.

To avoid the above problems, we move from the ALS-based method to the rank minimization method. Before the employment of later approach, the relationship between TR rank and TR unfolding rank is of critical importance. It is not difficult to discover that the rank of any TT unfolding $\mathbf{X}_{[k]} \in \mathbb{R}^{\prod_{i=1}^k n_i \times \prod_{i=k+1}^d n_i}$, $i \in \{1, \dots, d\}$ is r_k ($[r_1, \dots, r_{d-1}]^T$ is the TT rank), but it is not easy to give a clear characterization to the rank of TR unfolding. This lack of comprehension spurs us to have a deeper investigation to TR decomposition. Our contributions are itemized as follows:

- 1) Despite the computation of TR rank being obstructed by the cycle, we find and prove the relation between TR rank and TR unfolding's rank.
- 2) We analyze the sampling conditions for low rank tensor completion based on TR decomposition and give a sampling theorem for successful recovery. Based on it, a balanced unfolding's rank is gained to construct the rank minimization.
- 3) We use an alternating direction method of multipliers (ADMM) to solve the relaxed rank minimization problem, and the algorithmic complexity is analyzed. The experiments show the benefit of balance accommodated in the proposed algorithm.

The organization for the remainder of this paper is arranged as follows. In section II, the basic notations and preliminaries of TR are introduced. In section III, we mainly study the TR unfolding matrix from two perspectives, namely the equivalence of TR decomposition and singular value decomposition (SVD) of TR unfolding, along with a sampling theorem for low rank tensor completion based on TR decomposition. Some auxiliary theorems for convenient analysis and realization of algorithm are provided. In section IV, the balanced unfoldings are chosen to model the rank minimization. The TRBU is proposed to accomplish the tensor completion. Moreover, we analyze the algorithmic complexity. Section V provides the experimental results. Finally we conclude our work in section VI.

II. NOTATIONS AND PRELIMINARIES

A. Notations about tensor ring decomposition

This section introduces some basic notations of tensors. A scalar, a vector, a matrix and a tensor are denoted by normal letter, boldface lowercase letter, boldface uppercase letter and calligraphic letter, respectively. More specifically, a d -order

tensor is denoted as $\mathcal{X} \in \mathbb{R}^{n_1 \times \dots \times n_d}$, where n_i is the size corresponds to mode i , $i \in \{1, \dots, d\}$. An entry of the tensor \mathcal{X} is denoted as $x_{j_1 \dots j_d}$, where j_i is the index with mode i , $1 \leq j_i \leq n_i$ for any $i \in \{1, \dots, d\}$. A mode- k fiber of \mathcal{X} can be denoted as $\mathbf{x}_{j_1 \dots j_{k-1} j_k+1 \dots j_d}$, and $\mathbf{X}_{j_1 \dots j_{k-1} j_k+2 \dots j_d}$ represents the slice along mode k and mode $k+1$.

$\|\mathbf{X}\|_2 = \sigma_{\max}(\mathbf{X})$ denotes the spectral norm of the matrix \mathbf{X} , which is equal to its maximal singular value. Besides, we regard \mathbf{E} as the identity matrix.

The Frobenius norm of a tensor \mathcal{X} can be defined as follows:

$$\|\mathcal{X}\|_{\text{F}} = \sqrt{\sum_{j_1=1}^{n_1} \dots \sum_{j_d=1}^{n_d} x_{j_1 \dots j_d}^2}. \quad (1)$$

The inner product of two tensors \mathcal{X} and \mathcal{Y} is defined as

$$\langle \mathcal{X}, \mathcal{Y} \rangle = \sqrt{\sum_{j_1=1}^{n_1} \dots \sum_{j_d=1}^{n_d} x_{j_1 \dots j_d} y_{j_1 \dots j_d}}. \quad (2)$$

If $\mathbf{X} \in \mathbb{R}^{M \times N}$ and $\mathbf{Y} \in \mathbb{R}^{P \times Q}$, the Kronecker product can be written as follows:

$$(\mathbf{X} \otimes \mathbf{Y})_{ij} = x_{mp} \cdot y_{nq}, \quad (3)$$

where $i = m + (p-1)M$ and $j = n + (q-1)N$ for $m \in \{1, 2, \dots, M\}$, $n \in \{1, 2, \dots, N\}$, $p \in \{1, 2, \dots, P\}$ and $q \in \{1, 2, \dots, Q\}$.

The Hadamard product \circledast is an element-wise product, e.g., $(\mathbf{X} \circledast \mathbf{Y})_{ij} = x_{ij} y_{ij}$.

The rank R of a matrix \mathbf{X} can be represented as $R = \text{rank}(\mathbf{X})$, where $\text{rank}(\cdot)$ is the rank function of a matrix.

Mode- k unfolding maps a tensor to a matrix $\mathbf{X}_{(k)} \in \mathbb{R}^{n_k \times J}$ by rearranging the fibers as the columns of the matrix. i.e., $x_{j_1 \dots j_d} = x_{j_n j}$, and $j = \overline{j_1 \dots j_{k-1} j_{k+1} \dots j_d}$ is

$$j = 1 + \sum_{i=1, i \neq k}^d (j_i - 1) \prod_{m=1, m \neq k}^{i-1} n_m. \quad (4)$$

Mode- k matricization unfolds a tensor along its first k modes [34], i.e., $\mathbf{X}_{[k]} \in \mathbb{R}^{\prod_{i=1}^k n_i \times \prod_{i=k+1}^d n_i}$.

In the context of TR decomposition, $\mathbf{X}_{\{k,l\}}$ denotes the k -shifting l -matricization of the tensor \mathcal{X} . It firstly permutes the tensor with order $[k, \dots, d, 1, \dots, k-1]$ and performs matricization along first l modes.

As a special case of k -shifting l -matricization, k -shifting balanced unfolding $\mathbf{X}_{\langle k \rangle} \in \mathbb{R}^{n_k \dots n_{k-1+\zeta_k} \times n_{k+\zeta_k} \dots n_d \cdot n_1 \dots n_{d-1}}$ permutes a tensor with order $[k, \dots, d, 1, \dots, k-1]^T$ and unfolds tensor along its first ζ_k modes, where ζ_k is the k -th equilibrium number such that $\mathbf{X}_{\langle k \rangle}$ has the nearest size. The indices of $(\mathbf{X}_{\langle k \rangle})_{pq}$ can be formulated as

$$p = 1 + \sum_{i=k}^{k-1+d/2} (j_i - 1) \prod_{m=k}^{i-1} n_m \quad (5)$$

$$q = 1 + \sum_{i=k+d/2}^{k-1} (j_i - 1) \prod_{m=k+d/2}^{i-1} n_m.$$

Let $\{\mathcal{G}\} = \{\mathcal{G}^{(1)}, \dots, \mathcal{G}^{(d)}\}$ denote the cores of TR decomposition and the TR rank is $[r_1, \dots, r_N]^T$, where $\mathcal{G}^{(n)} \in$

$\mathbb{R}^{r_k \times n_k \times r_{k+1}}$. Then the scalar form of TR decomposition can be written as

$$x_{j_1 \dots j_d} = \sum_{t_1=1}^{r_1} \dots \sum_{t_d=1}^{r_d} g_{t_1 j_1 t_2}^{(1)} \dots g_{t_{d-1} j_{d-1} t_d}^{(d-1)} g_{t_d j_d t_1}^{(d)}. \quad (6)$$

Equivalently, it can be represented by a more compact form:

$$x_{j_1 \dots j_d} = \text{tr} \left(\mathbf{G}_{j_1}^{(1)} \dots \mathbf{G}_{j_d}^{(d)} \right), \quad (7)$$

where $\mathbf{G}_{j_k}^{(k)}$ is the j_k -th mode-2 slice of core $\mathcal{G}^{(k)}$, and $\text{tr}(\mathbf{X})$ is the trace of the matrix \mathbf{X} . There is a tensorized representation whose formulation is

$$\mathcal{X} = \sum_{t_1=1}^{r_1} \dots \sum_{t_d=1}^{r_d} \mathbf{g}_{t_1 t_2}^{(1)} \circ \dots \circ \mathbf{g}_{t_{d-1} t_d}^{(d-1)} \circ \mathbf{g}_{t_d t_1}^{(d)}. \quad (8)$$

where $\mathbf{g}_{t_k t_{k+1}}^{(k)}$ is the (t_k, t_{k+1}) -th mode-2 fiber of core $\mathcal{G}^{(k)}$, and \circ denotes the outer product.

We use $\overline{\otimes}$ to denote the tensor connection product. It combines several cores of TR into a new core and the formula is as below.

$$\left(\overline{\otimes}_{n=a}^b \mathcal{G}^{(k)} \right)_{t_a:t_{b+1}} = \sum_{t_{a+1}=1}^{r_a} \dots \sum_{t_b=1}^{r_b} \mathbf{g}_{t_a t_{a+1}}^{(a)} \otimes \dots \otimes \mathbf{g}_{t_b t_{b+1}}^{(b)}, \quad (9)$$

where $\overline{\otimes}_{n=a}^b \mathcal{G}^{(k)} \in \mathbb{R}^{r_a \times (\prod_{i=a}^b n_i) \times r_{b+1}}$.

B. Preliminaries

This subsection retrospects the classical tensor rank minimization methods for tensor completion. At present, the approaches of tensor completion via rank optimization are based on unfolding matrix completion, indeed. The formulation for matrix completion is [40]

$$\begin{aligned} & \min_{\mathbf{X}} \text{rank}(\mathbf{X}) \\ & \text{s. t. } \mathbf{X}_{\mathbb{O}} = \mathbf{T}_{\mathbb{O}}. \end{aligned} \quad (10)$$

Owing to the essence that the rank of a matrix takes discrete values (the combinatorical nature [34]), problem (10) is NP-hard. As a result, a convex relaxation of problem (10) is often considered as an efficient alternative [41]:

$$\begin{aligned} & \min_{\mathbf{X}} \|\mathbf{X}\|_* \\ & \text{s. t. } \mathbf{X}_{\mathbb{O}} = \mathbf{T}_{\mathbb{O}}, \end{aligned} \quad (11)$$

in which $\|\mathbf{X}\|_* = \sum_{n=1}^{\text{rank}(\mathbf{X})} \lambda_n$ is the nuclear norm of a matrix \mathbf{X} , and λ_n is the n -th singular value.

Following this routine, the conventional tensor rank (Tucker rank) minimization is formulated as a weighted sum of mode- k rank [7], [21]:

$$\begin{aligned} & \min_{\mathcal{X}} \sum_{k=1}^d \alpha_k \text{rank}(\mathbf{X}_{(k)}) \\ & \text{s. t. } \mathcal{X}_{\mathbb{O}} = \mathcal{T}_{\mathbb{O}}, \end{aligned} \quad (12)$$

whose solution is usually given by the following relaxation

[7], [21]:

$$\begin{aligned} & \min_{\mathcal{X}} \sum_{k=1}^d \alpha_k \|\mathbf{X}_{(k)}\|_* \\ & \text{s. t. } \mathcal{X}_{\mathbb{O}} = \mathcal{T}_{\mathbb{O}}, \end{aligned} \quad (13)$$

where $\mathbf{X}_{(n)}$ is the classical mode- k unfolding stemmed from Tucker decomposition.

In reference [34], the TT rank is defined as the rank of matricization $\mathbf{X}_{[k]}$ along k modes, which is

$$\begin{aligned} & \min_{\mathcal{X}} \sum_{k=1}^d \alpha_k \text{rank}(\mathbf{X}_{[k]}) \\ & \text{s. t. } \mathcal{X}_{\mathbb{O}} = \mathcal{T}_{\mathbb{O}}, \end{aligned} \quad (14)$$

problem (14) is tackled via optimization of TT nuclear norms [34], which is represented as below:

$$\begin{aligned} & \min_{\mathcal{X}} \sum_{k=1}^d \alpha_k \|\mathbf{X}_{[k]}\|_* \\ & \text{s. t. } \mathcal{X}_{\mathbb{O}} = \mathcal{T}_{\mathbb{O}}. \end{aligned} \quad (15)$$

As to the completion through HT rank minimization [37], the HT rank is represented by the rank of matricization along the nodes of tensor tree. The rank optimization can be characterized as

$$\begin{aligned} & \min_{\mathcal{X}} \sum_{q=1}^Q \alpha_q \text{rank}(\mathbf{X}^{(q)}) \\ & \text{s. t. } \mathcal{X}_{\mathbb{O}} = \mathcal{T}_{\mathbb{O}} \end{aligned} \quad (16)$$

if we disregard the term of total variation, where Q is the number of nodes. The convex relaxation of (16) is [37]

$$\begin{aligned} & \min_{\mathcal{X}} \sum_{q=1}^Q \alpha_q \|\mathbf{X}^{(q)}\|_* \\ & \text{s. t. } \mathcal{X}_{\mathbb{O}} = \mathcal{T}_{\mathbb{O}}. \end{aligned} \quad (17)$$

One may find that all the tensor completions via rank optimization is based on some particular unfolding matrices. However, this situation changes in the sense that the computation of TR rank is tricky. In the next section, we argue that TR rank minimization can be converted into other rank optimization model, and we show the most useful TR unfoldings are the balanced ones, which capture more global correlations than its analogues, i.e., TT unfoldings.

III. SAMPLING FOR LOW RANK TENSOR COMPLETION VIA TENSOR RING

This section consists of theories that are necessary for building the sampling scheme of our completion model.

Lemma 1 (TR matricization). *Consider a (sub-)critical TR then, for any $k \in \{1, \dots, d\}$, the k -shifting mode- l matricization $\mathbf{X}_{\{k,l\}}$ has unique singular vectors (tensors) and singular values.*

Remark. *The proof of Lemma 1 directly gives the formula of SVD expression for all $\mathbf{X}_{\{k,l\}}$ s, but note that this is not the standard SVD, since the singular vectors (tensors) are not*

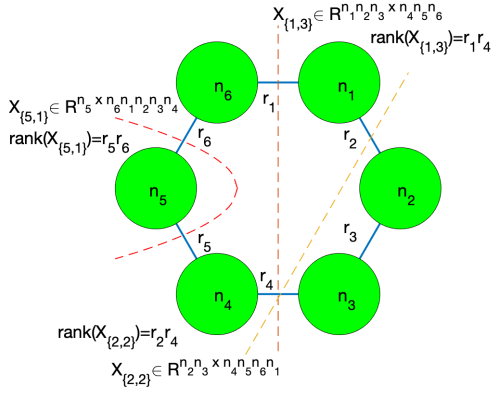


Fig. 1. An intuitive illustration of TR rank and its unfolding's rank, in which the 6-order tensor is with the size of $n_1 \times \dots \times n_6$, and its TR rank is $[r_1, \dots, r_6]^T$. The dashed lines represent the unfolding processing.

normalized due to the accumulative effect, this result can be seen in the proof of Theorem 1.

A useful conclusion can be derived from Lemma 1 is the relationship between TR rank and TR unfolding's rank, which can be characterized as follows. Fig. 1 gives a conceptual exhibition of Corollary 1. In the following a (sub-)critical TR is abbreviated to TR for concision wherever it appears.

Corollary 1 (TR unfolding's rank). *The rank of TR unfolding $\mathbf{X}_{\{k,l\}}$ is $\text{rank}(\mathbf{X}_{\{k,l\}}) = r_k r_{k+l}$, provided that the TR rank is $[r_1, \dots, r_d]^T$, where $k \in \{1, \dots, d\}$ and $l \in \{1, \dots, d-1\}$.*

Lemma 2 (McDiarmid inequality [42]). *Let $\{X_1, \dots, X_n\}$ be independent random variables such that for all i there is*

$$\begin{cases} a_i \leq X_i \leq b_i \\ c_i := b_i - a_i \\ \forall i : c_i \leq C \end{cases}$$

Let S be an arbitrary (implicit) function of the variables, e.g., the sum function, then for any $t > 0$ there is

$$P(|S - E(S)| > t) < 2e^{-\frac{2t^2}{nC^2}}, \quad (18)$$

as long as this function changes in a bounded way, i.e., if X_i is changed, the value of this function changes by at most $b_i - a_i < C$.

We build the TR strong incoherence property as depicted in Definition 1, which is crucial for the next theories and exact recovery guarantee.

Definition 1 (TR strong incoherence property). *Define a d -order tensor $\mathcal{X} \in \mathbb{R}^{n_1 \times \dots \times n_d}$ obeying the TR strong incoherence property with parameter $\mu = [\mu_1, \dots, \mu_d]^T$, $\mu \succ 0$ if for any $k \in \{1, \dots, d\}$,*

$$|\langle \mathcal{G}_{i_k \cdot}^{(k)}, \mathcal{G}_{\cdot j_k \cdot}^{(k)} \rangle - \frac{r_k r_{k+1}}{n_k} \mathbf{1}_{i_k=j_k}| \leq \frac{\mu_k \sqrt{r_k r_{k+1}}}{n_k}. \quad (19)$$

Theorem 1. *Suppose a d -order tensor $\mathcal{X} \in \mathbb{R}^{n_1 \times \dots \times n_d}$ is TR strong incoherent with parameter μ , then there are μ'_k and*

μ'' ($k = 1, 2, \dots$) such that

$$\begin{cases} |\langle \mathcal{U}_{i \cdot}, \mathcal{U}_{j \cdot} \rangle - \frac{r_n r_{n+l}}{\prod_{k=n}^{n+l-1} n_k} \mathbf{1}_{i=j}| \leq \frac{\mu'_{1nl} \sqrt{r_n r_{n+l}}}{\prod_{k=n}^{n+l-1} n_k} \\ |\langle \mathcal{V}_{i \cdot}, \mathcal{V}_{j \cdot} \rangle - \frac{r_n r_{n+l}}{\prod_{k=n+l}^{n-1} n_k} \mathbf{1}_{i=j}| \leq \frac{\mu'_{2nl} \sqrt{r_n r_{n+l}}}{\prod_{k=n+l}^{n-1} n_k} \end{cases} \quad (20)$$

and

$$|\langle \mathcal{U}_{i \cdot}, \mathcal{V}_{j \cdot} \rangle| \leq \frac{\mu'' \sqrt{r_n r_{n+l}}}{\sqrt{\prod_{k=1}^d n_k}} \quad (21)$$

hold with large probability, where

$$\begin{cases} \mathcal{U} = \prod_{k=n+1}^{n+l-1} \frac{1}{r_k} \otimes_{k=n}^{n+l-1} \mathcal{G}^{(k)} \\ \mathcal{V} = \prod_{k=n+l+1}^{n-1} \frac{1}{r_k} \otimes_{k=n+l}^{n-1} \mathcal{G}^{(k)} \end{cases} \quad (22)$$

are folded standard orthonormal bases. Here $p + q = d$.

Remark. Theorem 1 affirms that for any unfolding operation, i.e., arbitrary p and q such that $p + q = d$, one can always find a parameter $\mu_{nl} = \max\{\mu'_{1nl}, \mu'_{2nl}, \mu''\}$ such that μ'_{nl} and μ'' are less than or equal to μ_k , i.e., unfolding $\mathbf{X}_{\{n,l\}}$ satisfies the strong incoherence property, where

$$\begin{cases} \mu'_{1nl} = O\left(\prod_{k=n}^{n+l-1} \mu_{B_k} \sqrt{\sum_{k=n}^{n+l-1} \ln n_k}\right) \\ \mu'_{2nl} = O\left(\prod_{k=n+l}^{n-1} \mu_{B_k} \sqrt{\sum_{k=n+l}^{n-1} \ln n_k}\right) \\ \mu'' = \prod_{k=1}^d \mu_{B_k} \end{cases} \quad (23)$$

As a result, there is a parameter $\mu = \max_n \max_l \{\mu_{nl}\}$ such that all unfoldings $\mathbf{X}_{\{n,l\}}$ satisfy the strong incoherence property.

Recall \mathcal{U} and \mathcal{V} defined as (22), the standard SVD of any TR unfolding deduced from Theorem 1 is

$$\mathbf{X}_{\{n,l\}} = \mathcal{U}_{(2)'} \left(\prod_{k \neq n, n+l} r_k \text{tr}(\Sigma_k) \Sigma_n \otimes \Sigma_{n+l} \right) \mathcal{V}_{(2)}^T.$$

Lemma 3 (Matrix completion [41]). *Under the hypotheses of matrix strong incoherence property, and define $n := \max(n_1, n_2)$. There is a numerical constant C such that if*

$$m \geq C \mu^2 n r \ln^6(n), \quad (24)$$

then \mathbf{M} is the unique solution to (11) with probability at least $1 - n^{-3}$.

Theorem 2 (TR completion, uniformly bounded model). *Let the d -order tensor $\mathcal{X} \in \mathbb{R}^{n_1 \times \dots \times n_d}$ be sampled from a uniformly bounded model with TR rank being $[r_1, \dots, r_d]^T$. Under the hypotheses of Definition 1, define $n_l := \max\left\{\prod_{k=n}^{n+l-1} n_k, \prod_{k=n+l}^{n-1} n_k\right\}$. There is a numerical*

constant C such that if

$$m \geq C\mu^2 n_l r_n r_{n+l} \ln^6(n_l), \quad (25)$$

then \mathcal{X} is the unique solution to (30) with probability at least $1 - n_l^{-3}$, where μ is determined by the maximal value of (23).

Remark. The lower sampling bound of tensor completion based on TR has been established by Theorem 2, which is based on the unfolding matrices of TR. Note that when $d = 2$, the results of tensor completion based on TR becomes the standard matrix completion, one can regard r^2 as the matrix rank.

By leveraging Lemma 4, a good strategy to improve the lower bound is to set $l = \lceil d/2 \rceil$, though this behavior has a mild decrement on probability of successful recovery. Note that this is also a balanced choice, since it captures the mutual information between the half modes and the other half modes of a tensor, which can be easily proved using the technique introduced in [34]. Hence the balanced unfoldings offer more global information than the unbalanced ones. Accordingly, this choice induces the lowest number of observations among all other choices, which reveals the advantage of choosing balanced unfoldings from the perspective of sample complexity.

According to Lemma 1 and Theorem 1, a (sub-)critical TR decomposition is equivalent to many standard SVDs and any unfolding matrix that belongs to TR manifold is equivalent to TR theoretically, which turns out that TR decomposition does not need a ring and TR completion does not rely on TR decomposition. In fact, there is a similar conclusion that tensor tree decomposition does not need a tree too [43].

Lemma 4. Assume an N -way vector $\mathbf{x} \succ 1$ satisfies $||\mathbf{x}||_1 - \sqrt{N}||\mathbf{x}||_2 \leq \epsilon$, $|\beta/\alpha - 1|$ is minimal when $n = \lceil N/2 \rceil + \delta$, where $\alpha = \prod_{i=1}^n x_i$, $\beta = \prod_{i=n+1}^N x_i$ and δ is a small integer, i.e., $0, \pm 1, \pm 2, \dots$.

Remark. In practice, the dimensional sizes of a tensor are often different, and Lemma 4 shows the employment $r_{\text{bf}}^{(k)} = r_k \cdot r_{k+\lceil d/2 \rceil + \delta}$ is a good strategy, where the value of δ is set to 0 in algorithm for convenience.

IV. LOW RANK TENSOR COMPLETION METHOD

Throughout this paper, we consider the general tensor completion in the noiseless case. The first subsection is the deduction of our completion model. The algorithm is given in the second subsection and the following subsections contain the algorithmic analysis and convergence.

A. Balanced unfolding's rank minimization for tensor completion

Based on the conventional tensor rank minimization model [7], [11], [21], [28], [30], [34], here we also simply define the TR rank (assume the TR rank is $[r_1, \dots, r_d]^T$) minimization as follows, in which the weighted ℓ_1 norm of TR rank is optimized:

$$\begin{aligned} \min_{\mathcal{X}} \sum_{k=1}^d \alpha_k r_k \\ \text{s. t. } \mathcal{X}_{\mathbb{O}} = \mathcal{T}_{\mathbb{O}}, \end{aligned} \quad (26)$$

where $\mathcal{X}_{\mathbb{O}}$ is the projection of \mathcal{X} on the observation set \mathbb{O} , and α_k is the weight. The constraint requires that $x_{j_1 \dots j_d} = t_{j_1 \dots j_d}$ for all $(j_1, \dots, j_d) \in \mathbb{O}$.

Note that TR rank minimization (26) is intractable, because it is not only NP-hard as rank optimization, but also can not be computed due to the cyclic structure of TR, i.e., the r_n in (26) can not be explicitly formulated as the rank function of a matrix. Then Lemma 1 is proposed to bypass the aforementioned problem, from which we find that the TR rank minimization can be transformed to an optimization of TR unfolding's rank.

As claimed in remark of Lemma 1, there is always a product of two TR ranks equal to the rank of an unfolding matrix $\mathbf{X}_{\{k,l\}}$. Therefore, the minimization of TR rank can be realized by minimizing the unfolding's ranks. We name r_f as folded rank, because when unfolding the TR, the ranks seem to be folded intuitively according to Lemma 1. One should note that two TR networks with equal sum of ranks do not have a same state in general. For a tensor $\mathcal{X} \in \mathbb{R}^{n_1 \times \dots \times n_d}$ with TR-rank $[r_1, \dots, r_d]^T$, the degree of freedom (df) of the TR is [39]

$$\text{df}_{\text{TR}} = \sum_{i=1}^d r_i r_{i+1} n_i - \sum_{i=1}^d r_i^2 + 1,$$

where $r_{N+1} = r_1$.

Considering there are $\binom{d}{2} = d(d-1)/2$ folded ranks, or equivalently, the unfolding matrices, the transformation of TR rank optimization can be modeled as:

$$\begin{aligned} \min_{\mathcal{X}} \sum_{i=1}^{\frac{d(d-1)}{2}} w_i r_f^{(i)} \\ \text{s. t. } \mathcal{X}_{\mathbb{O}} = \mathcal{T}_{\mathbb{O}}. \end{aligned} \quad (27)$$

where w_i ($i = 1, \dots, d$) is the weights. Let $\mathbb{U}_i = \{k, l\}$ be the unfolding index that corresponds to the i -th TR unfolding matrix, then the relaxation of (27) is

$$\begin{aligned} \min_{\mathcal{X}} \sum_{i=1}^{\frac{d(d-1)}{2}} w_i \|\mathbf{X}_{\mathbb{U}_i}\|_* \\ \text{s. t. } \mathcal{X}_{\mathbb{O}} = \mathcal{T}_{\mathbb{O}}, \end{aligned} \quad (28)$$

However, there are too many minimizers in model (27). Obviously, it is unwise to blindly use all these matrices, since all their information included together are redundant while (27) suffers from a high computational complexity yet. Considerable unfolding matrices resulting from the cycle makes it hard to choose the more valuable ones. Hence we resort to a sampling theorem for low rank tensor completion based TR in preliminary to obtain the best choices. According to the remark of Theorem 2, the balanced unfolding matrix contains the most information, i.e., it captures the most global correlations of a tensor.

Lemma 1 proves that a TR is actually equivalent to all its unfolding matrices, and one balanced unfolding matrix owns one kind of global correlations [34]. For the sake of making most of abundant information hidden in TR, a natural consideration is to incorporate all balanced unfolding matrices. It is not hard to see that, to fully excavate these information,

we need at least $\lceil d/2 \rceil$ balanced unfoldings.

Suggested by the remark of Lemma 4, the balanced folded rank minimization is characterized as follows:

$$\begin{aligned} \min_{\mathcal{X}} \sum_{k=1}^{\lceil d/2 \rceil} w_k r_{\text{bf}}^{(k)} \\ \text{s. t. } \mathcal{X}_{\mathbb{O}} = \mathcal{T}_{\mathbb{O}}. \end{aligned} \quad (29)$$

Compared with the TR rank minimization, the balanced folded rank minimization can be solved in theory, but it still can not be solved in practice as a result of its NP-hardness caused by the essence that a rank of matrix takes discrete values. One reasonable method is to resort to convex relaxation. Since nuclear norm is the tightest convex hull of matrix rank, we derive the following model based on the remark of Lemma 1.

The nuclear norm of an unfolding matrix associated with the k -th balanced folded rank $r_{\text{bf}}^{(k)}$ is $\|\mathbf{X}_{(k)}\|_*$, and the corresponding optimization model can be formulated as

$$\begin{aligned} \min_{\mathcal{X}} \sum_{k=1}^{\lceil d/2 \rceil} w_k \|\mathbf{X}_{(k)}\|_* \\ \text{s. t. } \mathcal{X}_{\mathbb{O}} = \mathcal{T}_{\mathbb{O}}. \end{aligned} \quad (30)$$

This proposed model has two main advantages. Form the model perspective, it has the lowest sample complexity among all unfolding choices, as stated in remark of Theorem 2. From an algorithm point of view, it results in lowest computational complexity, which is not hard to be seen from Lemma 4.

One may argue that model (30) is somewhat similar to (12) and (14) and (16), which seems to act on different unfolding matrices merely, i.e., FP-LRTC [21] utilizes classical mode- k unfoldings and SiLRTC-TT [34] adopts mode- k matricizations, while the k -shifting half unfoldings proposed in this paper are used instead. However, there is an essential difference behind this intuitive nuance. Concretely, the resulting completion model (30) is founded on the sampling theorem for low rank tensor completion bases on TR, model (12) is based on the low k -rank of Tucker decomposition, model (14) is valid owing to its achievement of capturing more global correlation than conventional mode- k unfolding, the effectiveness of model (16) is because of the low-rank of hierarchical Tucker decomposition. Furthermore, it has been shown that the k -shifting balanced unfolding can provide more global information than mode- k matricization (Theorem 2), which we will see in the experiments later.

B. Algorithm

In order to solve model (30), we substitute \mathbf{M}_k for $\mathbf{X}_{(k)}$ to get rid of interdependence and derive the following model:

$$\begin{aligned} \min_{\mathbf{M}_k} \sum_{k=1}^{\lceil d/2 \rceil} w_k \|\mathbf{M}_k\|_* \\ \text{s. t. } \mathcal{X}_{\mathbb{O}} = \mathcal{T}_{\mathbb{O}} \\ \mathbf{M}_k = \mathbf{X}_{(k)} \quad (k = 1, \dots, \lceil d/2 \rceil), \end{aligned} \quad (31)$$

where \mathbf{M}_k ($k = 1, \dots, \lceil d/2 \rceil$) are matrix variables. Considering the augmented Lagrangian function of (31) as follows:

$$\begin{aligned} \min_{\mathbf{M}_k, \mathbf{X}, \mathbf{Y}_k} \sum_{k=1}^{\lceil d/2 \rceil} (w_k \|\mathbf{M}_k\|_* + \langle \mathbf{M}_k - \mathbf{X}_{(k)}, \mathbf{Y}_k \rangle) \\ + \frac{\mu}{2} \|\mathbf{M}_k - \mathbf{X}_{(k)}\|_F^2 \\ \text{s. t. } \mathcal{X}_{\mathbb{O}} = \mathcal{T}_{\mathbb{O}}, \end{aligned} \quad (32)$$

which can be rewritten as

$$\begin{aligned} \min_{\mathcal{M}^{(k)}, \mathcal{X}, \mathcal{Y}^{(k)}} \sum_{k=1}^{\lceil d/2 \rceil} (w_k \|\mathcal{M}_{(k)}^{(k)}\|_* + \langle \mathcal{M}^{(k)} - \mathcal{X}, \mathcal{Y}^{(k)} \rangle) \\ + \frac{\mu}{2} \|\mathcal{M}^{(k)} - \mathcal{X}\|_F^2 \\ \text{s. t. } \mathcal{X}_{\mathbb{O}} = \mathcal{T}_{\mathbb{O}}, \end{aligned} \quad (33)$$

in which $\mathcal{M}^{(k)} = (\mathbf{M}_k)_{(k)-1} = \text{fold}_k(\mathbf{M}_k)$.

According to the framework of ADMM, the updating scheme is determined by

$$\begin{cases} \{\mathcal{M}\} = \arg \min_{\{\mathcal{M}\}} L_\mu(\{\mathcal{M}\}, \mathcal{X}, \{\mathcal{Y}\}) \\ \mathcal{X} = \arg \min_{\mathcal{X}} L_\mu(\{\mathcal{M}\}, \mathcal{X}, \{\mathcal{Y}\}) \\ \{\mathcal{Y}\} = \{\mathcal{Y}\} + \mu(\{\mathcal{M}\} - \mathcal{X}) \end{cases} \quad (34)$$

where L_μ is the objective function in (33).

The details about the ADMM algorithm for TR rank minimization are summarized in Algorithm 1.

Algorithm 1 Low TR-rank Tensor Completion via Balanced Unfolding (TRBU)

Input: Zero-filled observed tensor \mathcal{T} , observation set \mathbb{O} , penalty coefficient μ , number of maximal iterations K .

Output: Recovered tensor \mathcal{X} .

- 1: Initialization $\mathcal{X}_0 = \mathcal{T}$, $\{\mathcal{M}\} = \mathcal{X}_0$, $\{\mathcal{Y}\} = \mathcal{O}$.
- 2: **for** $k = 1$ **to** K **do**
- 3: **for** $i = 1$ **to** $\lceil d/2 \rceil$ **do**
- 4: $\mathcal{M}^{(i)} = \text{fold}_i(\mathbf{D}_{w_i/\mu}(\mathcal{X}_{(i)} - \mathcal{Y}_{(i)}^{(i)})/\mu)$
- 5: **end for**
- 6: $\mathcal{X}_{\mathbb{O}^c} = \frac{1}{\lceil d/2 \rceil} \sum_{i=1}^{\lceil d/2 \rceil} (\mathcal{M}^{(i)} + \mathcal{Y}^{(i)})/\mu$
- 7: **for** $i = 1$ **to** $\lceil d/2 \rceil$ **do**
- 8: $\mathcal{Y}^{(i)} = \mathcal{Y}^{(i)} + \mu(\mathcal{M}^{(i)} - \mathcal{X})$
- 9: **end for**
- 10: **end for**
- 11: **return** \mathcal{X}

In Algorithm 1, $\mathbf{D}_\gamma(\cdot)$ is a matrix shrinkage operator that truncates the singular value matrix by threshold γ , whose definition is $\mathbf{D}_\gamma(\mathbf{M}) = \mathbf{U} \mathbf{S}_\gamma(\mathbf{\Sigma}) \mathbf{V}^T = \mathbf{U} \text{diag}(\boldsymbol{\sigma}) \mathbf{V}^T$ [44]. Here $\mathbf{S}_\gamma(\mathbf{\Sigma}) := \mathbf{S}_\gamma(\boldsymbol{\sigma})$, of which the scalar form is

$$\mathbf{S}_\gamma(\sigma_r) = \begin{cases} \sigma_r - \gamma & (\sigma_r > \gamma) \\ 0 & (\sigma_r \leq \gamma) \end{cases}.$$

C. Algorithmic complexity

For a d -order hypercube tensor $\mathcal{X} \in \mathbb{R}^{n \times \dots \times n}$, the complexity of TRBU algorithm mainly comes from thresholding the

singular values. Every iteration contains $d/2$ soft thresholdings which has complexity $O(n^{3d/2})$, accordingly one iteration has complexity $O(dn^{3d/2}/2)$. One strategy is to find a substitution for the computation of SVD. References [12] and [21] mention the Lanczos algorithm is a good counterpart which has a linear time complexity $O(p+q)$ for a p -by- q matrix. Therefore, the overall computational complexity of TRBU is $O(dn^{d/2})$.

Unlike the ALS method compresses a tensor into a TR with dnr^2 parameters, the storage complexity of TRBU algorithm is $n^{d/2+1}r^2$, since $d/2$ outcomes of SVDs are stored instead.

D. Algorithmic convergence

The ADMM algorithm has a linear rate of convergence when one of the objective terms is strongly convex [45]. Reference [46] provides a rather simple but efficient strategy to improve convergence, in which the penalty coefficient μ increases geometrically with iterations, i.e., $\mu_{k+1} = \beta\mu_k$, where β is a constant.

V. NUMERICAL EXPERIMENTS

In this section, three groups of datasets are used for tensor completion experiments, i.e., synthetic data, real-world images and videos. Seven algorithms are used to test the performance on real-world data, consisting of alternating least square for low rank tensor completion via tensor ring (TR-ALS) [36], simple low-rank tensor completion via tensor train (SiLRTC-TT) [34], high accuracy low rank tensor completion algorithm (HaLRTC) [7], low rank tensor completion via tensor nuclear norm minimization (LRTC-TNN) [47], Bayesian CP Factorization (FBCP) for image recovery [16], smooth low rank tensor tree completion (STTC) [37] and the proposed one. These methods come from different tensor decompositions, including CP, Tucker, t-SVD, HT, TT and TR. All the algorithms are based on rank minimization except FBCP and TR-ALS. Note that the FBCP is powerful among the CP-based methods, as it use fully Bayesian inference to automatically determine the CP rank and, the uncertainty information of latent factors are also taken into account [16]. TR-ALS is selected to be compared because it is the first TR-based method. All the experiments are conducted in MATLAB 9.3.0 on a computer with a 2.8GHz CPU of Intel Core i7 and a 16GB RAM.

There are several evaluations for the quality of visual data. Relative error (RE), short for the root of relative squared error, is a common indicator for recovery accuracy, which is defined as

$$RE = \|\hat{\mathcal{X}} - \mathcal{X}\|_F / \|\mathcal{X}\|_F, \quad (35)$$

where \mathcal{X} is the ground truth and $\hat{\mathcal{X}}$ is the recovered tensor.

The second quality metric is peak signal-to-noise ratio, often abbreviated PSNR, is the ratio between the maximum possible power of a signal and the power of corrupting noise [48]. Given the ground truth \mathcal{X} and the estimation $\hat{\mathcal{X}}$, the mean squared error (MSE) is defined as

$$MSE = \frac{\|\hat{\mathcal{X}} - \mathcal{X}\|_F^2}{\text{card}(\mathcal{X})}, \quad (36)$$

then the PSNR (in dB) is defined as

$$\text{PSNR} = 20 \lg \left(M / \sqrt{\text{MSE}} \right), \quad (37)$$

where M is the maximal pixel value which is 255 for the RGB images and videos, and $\text{card}(\cdot)$ represents the number of elements in a set. A higher PSNR usually indicates a higher quality of the reconstruction.

The third assessment is called structural similarity index (SSIM) which is used for measuring the similarity between the recovered image and original image [49]. It is calculated on various windows of an image. The measure between two windows X and Y of common size $N \times N$ is

$$\text{SSIM}_{XY} = \frac{(2\mu_X\mu_Y + c_1)(2\sigma_{XY} + c_2)}{(\mu_X^2 + \mu_Y^2 + c_1)(\sigma_X^2 + \sigma_Y^2 + c_2)}, \quad (38)$$

where μ_X and μ_Y are the averages of X and Y , σ_X and σ_Y are the variances of X and Y , $c_1 = (k_1 L)^2$ and $c_2 = (k_2 L)^2$ are two variables to stabilize the denominator (default values for k_1 and k_2 are 0.01 and 0.03), $L = 2^{\#\text{bits per pixel}} - 1$ is the dynamic range of pixel-values.

The last one quantifying the algorithmic complexity is the computational CPU time (in seconds).

The sampling ratio (SR) is defined as the ratio of the number of sampled entries to the number of the elements in tensor \mathcal{X} , noted as $\text{SR} = \text{card}(\mathcal{O}) / \text{card}(\mathcal{X})$.

For fair comparisons, the parameters in each algorithm are tuned to give optimal performance, and all trials are repeated adequate times for avoiding fortuitous results. In our algorithm, μ_0 is set to be 1×10^{-3} . The convergence is determined by the relative change (RC) $\text{RC} = \|\mathcal{X}_k - \mathcal{X}_{k-1}\|_F / \|\mathcal{X}_{k-1}\|_F$, where the tolerance is set to be 1×10^{-5} . The number of maximal iterations is 100.

In the rest of this section, we firstly verify the theoretic analysis using synthetic data. Then the experiments on real-world data including image and video are used to test the performance of the proposed TRBU algorithm and other methods.

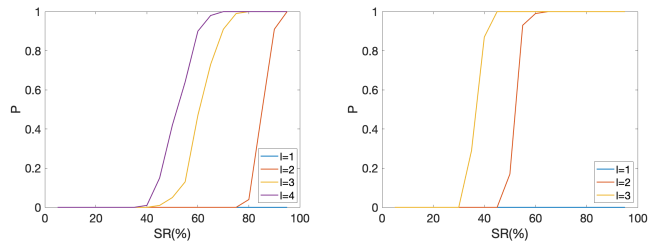
A. Synthetic data

We firstly consider a 5-order tensor $\mathcal{X} \in \mathbb{R}^{36 \times \dots \times 36}$ with TR rank being $[9, 2, 7, 5, 3]^T$. The entries of TR rank are prime numbers so that every product of two elements is different from others. The tensor is generated by TR decomposition, where core tensors $\{\mathcal{G}\}$ are with i.i.d. standard Gaussian random variables, i.e., $\mathcal{G}^{(n)}(r_n, i_n, r_{n+1}) \sim \mathcal{N}(0, 1)$, $n = 1, \dots, N$. Subsequently, it is unfolded into 20 different matrices $\mathbf{X}_{\{n,l\}}$, $n = 1, \dots, 5$, $l = 1, \dots, 4$, and we calculate their theoretic ranks r_t and real ranks r_f to validate Lemma 1. The results are put in Table I, which shows the correctness of this theory.

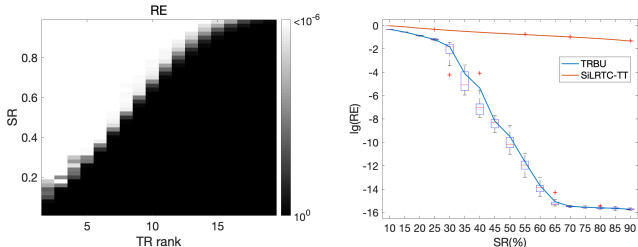
To testify Theorem 2, we simulate another two tensors, one is an 8-order tensor $\mathcal{X} \in \mathbb{R}^{3 \times \dots \times 3}$ with TR-rank 2, the other is a 6-order tensor $\mathcal{X} \in \mathbb{R}^{6 \times \dots \times 6}$ with TR-rank 3. The entries of core tensors are sampled independently from the standard normal distribution. Their SRs range from 5% to 95% with linear increment $\text{dSR} = 5\%$. For each tensor with different SRs we run the TRBU algorithm 100 times to recover its $N/2$

TABLE I
THE THEORETIC AND REAL RANKS OF TR UNFOLDING MATRICES
 $\mathbf{X}_{\{n,l\}}$, $n = 1, \dots, 5$, $l = 1, \dots, 4$.

Unfolding	r_t	r_f	Unfolding	r_t	r_f
$\mathbf{X}_{\{1,1\}}$	$r_1 r_2 = 18$	18	$\mathbf{X}_{\{3,3\}}$	$r_3 r_1 = 63$	63
$\mathbf{X}_{\{1,2\}}$	$r_1 r_3 = 63$	63	$\mathbf{X}_{\{3,4\}}$	$r_3 r_2 = 14$	14
$\mathbf{X}_{\{1,3\}}$	$r_1 r_4 = 45$	45	$\mathbf{X}_{\{4,1\}}$	$r_4 r_5 = 15$	15
$\mathbf{X}_{\{1,4\}}$	$r_1 r_5 = 27$	27	$\mathbf{X}_{\{4,2\}}$	$r_4 r_1 = 45$	45
$\mathbf{X}_{\{2,1\}}$	$r_2 r_3 = 14$	14	$\mathbf{X}_{\{4,3\}}$	$r_4 r_2 = 10$	10
$\mathbf{X}_{\{2,2\}}$	$r_2 r_4 = 10$	10	$\mathbf{X}_{\{4,4\}}$	$r_4 r_3 = 35$	35
$\mathbf{X}_{\{2,3\}}$	$r_2 r_5 = 6$	6	$\mathbf{X}_{\{5,1\}}$	$r_5 r_1 = 27$	27
$\mathbf{X}_{\{2,4\}}$	$r_2 r_1 = 18$	18	$\mathbf{X}_{\{5,2\}}$	$r_5 r_2 = 6$	6
$\mathbf{X}_{\{3,1\}}$	$r_3 r_4 = 35$	35	$\mathbf{X}_{\{5,3\}}$	$r_5 r_3 = 21$	21
$\mathbf{X}_{\{3,2\}}$	$r_3 r_5 = 21$	21	$\mathbf{X}_{\{5,4\}}$	$r_5 r_4 = 15$	15



(a) An 8-order tensor $\mathcal{X} \in \mathbb{R}^{3 \times \dots \times 3}$ with TR-rank $(2, \dots, 2)^T$. (b) A 6-order tensor $\mathcal{X} \in \mathbb{R}^{6 \times \dots \times 6}$ with TR-rank $(3, \dots, 3)^T$.



(c) The phase transition of tensor completion for a 4D tensor $\mathcal{X} \in \mathbb{R}^{20 \times \dots \times 20}$. (d) The box-plot regarding to REs versus SRs of a 4-order tensor $\mathcal{X} \in \mathbb{R}^{20 \times \dots \times 20}$. The solid lines are the mean values of the results.

Fig. 2. Three experiments on randomly generated data. The top two subfigures are the validation of balance in TR. The bottom left subfigure is used to testify the recovery guarantee in sampling theorem, and the bottom right one is a comparison of TR-based and TT-based algorithm.

unfolding matrices, i.e., $\mathbf{X}_{\{1,l\}}$, $l = 1, \dots, N/2$. The averaged results are shown in (a) and (b) within Fig. 2, which gives the recovery probabilities with respect to various SRs. In this experiment, the recovery is considered to be successful when $RE < 1 \times 10^{-6}$. It can be seen from the results that a balanced unfolding matrix is easier to recover than an unbalanced one, and the more balance of the unfolding the more ease of its completion. This verifies the correctness of remark of Theorem 2.

In order to verify the exact tensor completion guarantee in Theorem 2, we randomly generate a set of 4-order tensors $\mathcal{X} \in \mathbb{R}^{20 \times \dots \times 20}$ by contracting the cores $\{\mathcal{G}\}$, whose entries are sampled from an i.i.d. $\mathcal{N}(0, 1/20)$ distribution. The degree of freedom (df) of a balanced TR unfolding is



Fig. 3. The original copies of “kodim04”, “peppers”, “sailboat”, “lena”, “barbara”, “house”, “airplane” and “Einstein”, respectively.

$df_M = r^2 (2\sqrt{n^d} - r^2)$, and the df for a TR is $df_{TR} = dnr^2 - dr^2 + 1$. We choose TR rank from 2 to 19 so that df_M is ensured to be positive. For each tube (SR, TR rank), we repeat the completion 10 times. The phase transition of this tensor completion is given as Fig. 2(c), in which a recovery is regarded as a successful completion if $RE < 1 \times 10^{-6}$. From Fig. 2(c), a large amount of region is successfully recovered, the results in is a convincing validation of the recovery guarantee in Theorem 2. The phenomenon in Fig. 2(c) also implies that there is a tighter bound of tensor completion based on TR, since the starting point of bound in this paper is based on unfolding matrix, instead of the TR itself.

The last Fig. 2(d) gives the logarithm of RE to the base 10, in which the SR increases linearly from 0.1 to 0.9. Note that the tensor for TRBU is generated by TR decomposition and the tensor for SiLRTC-TT is generated by tensor train decomposition, both tensor has a same size $\mathbb{R}^{20 \times 20 \times 20 \times 20}$. The TR rank is $[2, 2, 2, 2]^T$ and the TT rank is $[2, 2, 2]^T$. The results are at an average of 20 trials for TRBU with TR-rank $[2, 2, 2, 2]^T$, SiLRTC-TT with TT-rank $[2, 2, 2]^T$. TRBU always has the lowest RE compared with SiLRTC-TT. With increasing SR, the RE of TRBU drops drastically while SiLRTC-TT's decreases slowly, which demonstrates the inefficiency of SiLRTC-TT. The results also indicate the correctness of Theorem 2, as it asserts the most “useful” unfolding matrices are the balanced ones. Many unfoldings of TT have “low values”, which results in a worse performance compared to the usage of TR's balanced unfoldings.

B. Color images

Eight RGB image are tested in this section's experiment, including “kodim04”¹, “peppers”, “sailboat”, “lena”, “barbara”, “house”, “airplane” and “Einstein” [36]. The original images are shown in Fig. 3. The displaying result of each image is based on an averaged of 10 experiments. The SRs for all the considered images are from 10% to 90%. In image recovery, we set $\beta = 1.028$.

¹<http://r0k.us/graphics/kodak/kodim04.html>

The visual data tensorization (VDT) method introduced in [34] and [50] can improve the performance, as a higher-order tensor makes it more efficient to exploit the local structures in original tensor and, if a tensor is slightly correlated, the tensorized one is more likely to have a low rank [34]. VDT first transforms an image into a real ket of a Hilbert space by casting the image to a higher-order tensor with an appropriate block structured addressing, i.e., tensorizing an image of size $M \times N \times 3$ to a tensor of size $m_1 \times \dots \times m_K \times n_1 \times \dots \times n_K \times 3$. Then VDT permutes and reshapes the resulting tensor into another one with size $m_1 n_1 \times \dots \times m_K n_K \times 3$. For the first image, we use $[2 * \text{ones}(1, 8), 3, 2 * \text{ones}(1, 9), 3]^T$ to reshape it and finally get a $[4 * \text{ones}(1, 8), 6, 3]^T$ sized tensor. For the second to the seventh images, we first reshape them into 17-order tensors with size of $2 \times \dots \times 2 \times 3$, then the outcomes are reshaped into $4 \times \dots \times 4 \times 3$ sized 9D tensors after the reordering. As to the last image, $[2, 2, 2, 3, 5, 5, 5, 3, 2, 2, 2, 3]^T$ and $[10, 10, 6, 6, 10, 10, 3]^T$ are the resulting orders during the VDT processing. Note that the tensorizations are manually operated, and different operations will cause other results.

After applying the VDT manipulation, we compare the proposed method with the state-of-the-art algorithms. The recovery results (REs, PSNRs, SSIMs and CPU times) of 7 algorithms, based on an average of 5 repetitions, are exhibited in Fig. 4. The FBCP method needs a pre-defined maximal CP rank, which limits the computational source very much. For instance, the given maximum CP ranks for “kodim04” and “Einstein” are 50 and 60 respectively, while 100 for others, otherwise the algorithm will be out of memory. The TR ranks for all images are both 14 in TR-ALS. The performances of TR-ALS does not improve too much with the increasing SR because of the fixed given TR rank. However, the computational complexity of TR-ALS (one can refer to [36]) increases rapidly with linearly enlarged TR rank, which will result in a large amount of time and greatly limit the performance of TR-ALS. From these results, the TRBU method prevails against all other tested algorithms on all evaluation metrics except for CPU time, which suggests the efficiency of the proposed method. Aside from the high CPU time of TR-ALS, all other three indicators are also much worse than TRBU’s. This implies the advantage of TRBU that it considers the completion problem from an information theory point of view. Although the closed loop of TR increases difficulty of TR rank minimization, it provides richer information compared with other tensor decomposition formats, which is a main reason why the better performances can be derived by TRBU.

Besides, we use text-masked “house” and palm-masked “llama” images to test the seven methods’ performances on the condition of nonuniform sampling. The maximal CP ranks for two images are both 100. The corresponding results are presented in Fig. 5, it can be concluded that TRBU is still superior to all other six methods in terms of recovery quality, i.e., RE, PSNR and SSIM, while keeping an acceptable CPU time.

C. Real-world videos

In this group of experiments, two videos are used to test the algorithms and each video recovery is tested 5 times. The

first is a color video called “explosion” ² with the size of $800 \times 1280 \times 3 \times 401$. We use the frames from the 81st to the 180th. Each frame is down-sampled to the size of $80 \times 128 \times 3$, the whole video is reshaped into a 9D tensor with the size of $8 \times 8 \times 4 \times 4 \times 10 \times 3 \times 4 \times 5 \times 5$ by VDT method. The second is a color video named “cock” ³ download from website. we down-sampled each frame to the size of $72 \times 128 \times 3$ and finally get a $8 \times 8 \times 4 \times 6 \times 6 \times 3 \times 4 \times 5 \times 5$ sized tensor. The SRs of both two videos are 10%. Furthermore, we set $\mu = 1.028$. The TR ranks for two videos are both 12.

Fig. 6 gives the completion results of seven methods. The maximal CP ranks are limited by 40 in the completions, which may deteriorate the performances of FBCP. This also implies the disadvantage of FBCP’s huge storage requirement. TR-ALS can not be able to effectively perform the resolutions, as the contractions of core tensors and calculations of inverse matrices cost too much time when the size of tensor is large. Among all the methods, the proposed TRBU has much better recovery quality for two experiments of video recovery.

VI. CONCLUSION

We study the TR rank and TR unfolding’s rank and, based on this foundation, we propose a lower bound for sampling for tensor completion via TR format. Motivated by the sampling theorem, we use the balanced unfoldings to build the weighted sum of nuclear norm minimization for tensor completion. We propose a TRBU algorithm for tensor completion. The numerical experiments demonstrate the enhancement of the proposed method’s performance on recovery quality.

APPENDIX A PROOF OF LEMMA 1

Proof. Considering a general generic TR representation of tensor \mathcal{X} , where d singular value matrices are inserted into d pairs of adjoint core tensors, i.e., Σ_{n+1} is inserted between core $\mathcal{G}^{(n)}$ and core $\mathcal{G}^{(n+1)}$.

We use a little trick to deal with this generality. Note that every mode-2 slice of core $\mathcal{G}^{(n)}$ has the same status when interacting with Σ_n and Σ_{n+1} , then a substitution for the aforementioned representation is $\tilde{\mathcal{G}}^{(n)} = \mathcal{W}^{(n)} \otimes \mathcal{G}^{(n)}$, where $\mathcal{W}_{:i_n:}^{(n)} = \text{diag}(\sqrt{\Sigma_n}) \text{diag}(\sqrt{\Sigma_{n+1}})^T$ holds for all mode-2 slices of $\mathcal{W}^{(n)}$. We use matrix $\mathbf{W}^{(n)}$ to denote the slice of $\mathcal{W}^{(n)}$ for convenience, as all its mode-2 slices are the same.

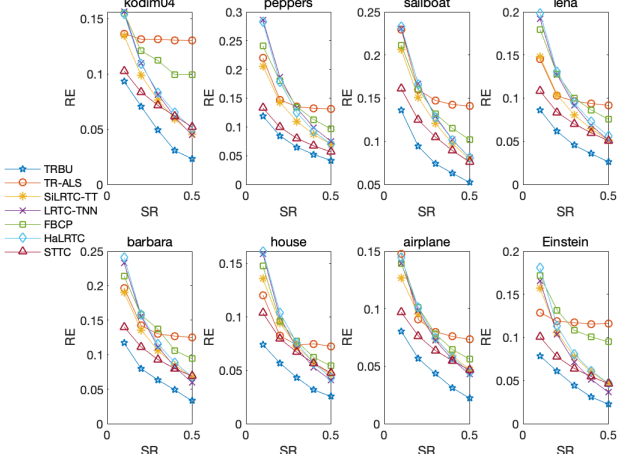
Suppose a 4-order tensor is considered and by the mathematic induction, we first aim to calculate the ℓ_2 -norm of the mode-2 fiber of $\tilde{\mathcal{G}}^{(1)} \otimes \tilde{\mathcal{G}}^{(2)}$. For simplicity, we denote by \mathbf{U} the r_1 -th mode-1 slice of $\tilde{\mathcal{G}}^{(1)}$ and \mathbf{V} the r_3 -th mode-3 slice of $\tilde{\mathcal{G}}^{(2)}$, respectively. Consequently the squared 2-norm is calculated by $\sum_i \sum_j (\mathbf{U} \mathbf{V}^T)_{ij}^2$, which can be rewritten as

$$\sum_k w_{r_1 k}^{(1)} w_{k r_3}^{(2)} \sum_t w_{r_1 t}^{(1)} w_{t r_3}^{(2)} \sum_i u_{ik} u_{it} \sum_j v_{jk} v_{jt}.$$

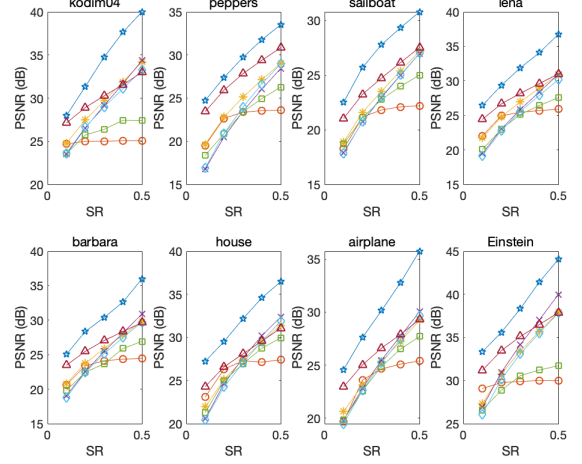
The above term can be simplified to $(\mathbf{W}^{(1)} \mathbf{W}^{(2)})_{r_1 r_3}^2$ using the orthonormal condition of \mathbf{U} and \mathbf{V} . Thus the

²<http://www.newcger.com/shipinsucai/5786.html>

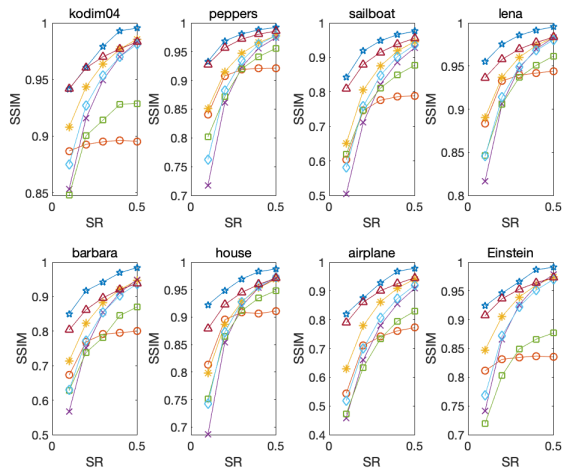
³<https://pixabay.com/videos/id-10685/>



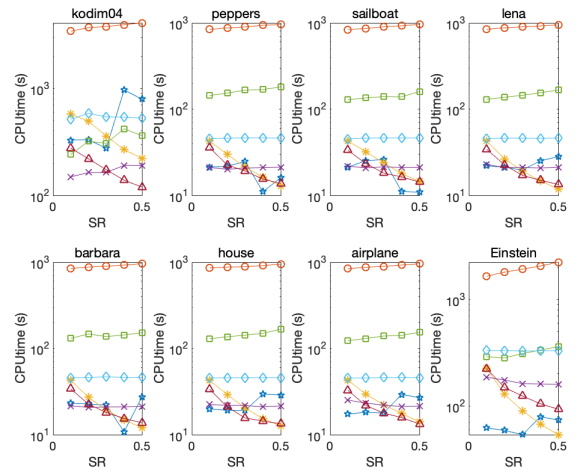
(a) Comparison of different algorithms on RE



(b) Comparison of different algorithms on PSNR



(c) Comparison of different algorithms on SSIM



(d) Comparison of different algorithms on CPU time

Fig. 4. Comparisons of 8 image recovery based on 7 algorithms, including 4 evaluation criteria: RE, PSNR, SSIM and computational CPU time.

norm of all the mode-2 fibers of $\tilde{\mathcal{G}}^{(1)} \otimes \tilde{\mathcal{G}}^{(2)}$ is $\mathbf{W}^{(1)} \mathbf{W}^{(2)} = \text{tr}(\Sigma_2) \text{diag}(\sqrt{\Sigma_1}) \text{diag}(\sqrt{\Sigma_3})^T$ and the reformulation for the unfolding is

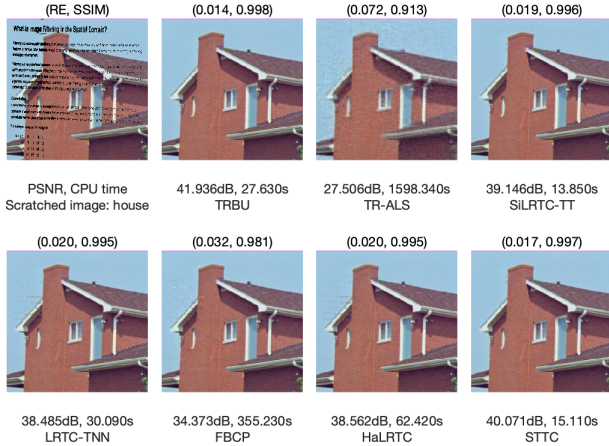
$$\mathbf{X}_{\{1,2\}} = \left[\left(\mathcal{W}^{(1)} \bar{*} \mathcal{W}^{(2)} \right) \otimes \mathcal{U} \right]_{(2)'} \left[\left(\mathcal{W}^{(3)} \bar{*} \mathcal{W}^{(4)} \right) \otimes \mathcal{V} \right]_{(2)}^T,$$

where $\bar{*}$ is the matrix product between corresponding mode-2 slices, $(\cdot)_{(2)'}^T$ unfolds a TR's core tensor into a matrix with permuted order $[2, 3, 1]^T$ and $(\cdot)_{(2)}^T$ unfolds a TR's core tensor into a matrix with order $[2, 1, 3]^T$. Thus the SVD of $\mathbf{X}_{\{1,2\}}$ can be denoted as

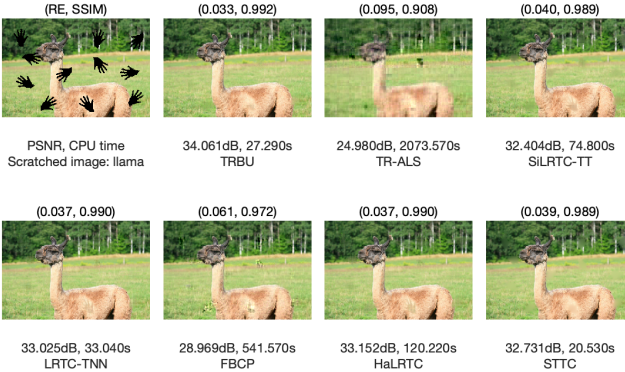
$$\mathbf{X}_{\{1,2\}} = \mathcal{U}_{(2)'} \Sigma (\mathcal{V}_{(2)})^T,$$

$$\begin{aligned} & \text{where } \mathcal{U} = \mathcal{G}^{(1)} \otimes \mathcal{G}^{(2)}, \mathcal{V} = \mathcal{G}^{(3)} \otimes \mathcal{G}^{(4)} \text{ and} \\ & \Sigma = \text{diag} \left(\overrightarrow{(\mathbf{W}^{(1)} \mathbf{W}^{(2)})} \right) \otimes \text{diag} \left(\downarrow (\mathbf{W}^{(3)} \mathbf{W}^{(4)}) \right) \\ & = \text{tr}(\Sigma_2) \text{diag} \left(\overrightarrow{\left(\text{diag}(\sqrt{\Sigma_1}) \text{diag}(\sqrt{\Sigma_3})^T \right)} \right) \otimes \\ & \quad \text{tr}(\Sigma_4) \text{diag} \left(\downarrow \left(\text{diag}(\sqrt{\Sigma_3}) \text{diag}(\sqrt{\Sigma_1})^T \right) \right) \\ & = \text{tr}(\Sigma_2) \text{tr}(\Sigma_4) \text{diag} \left(\downarrow \left(\sqrt{\sigma_3} \sqrt{\sigma_1}^T \right) \right) \otimes \\ & \quad \text{diag} \left(\downarrow \left(\sqrt{\sigma_3} \sqrt{\sigma_1}^T \right) \right) \\ & = \text{tr}(\Sigma_2) \text{tr}(\Sigma_4) \text{diag} \left((\sqrt{\sigma_1} \otimes \sqrt{\sigma_3}) \otimes (\sqrt{\sigma_1} \otimes \sqrt{\sigma_3}) \right) \\ & = \text{tr}(\Sigma_2) \text{tr}(\Sigma_4) \text{diag} (\sigma_1 \otimes \sigma_3) \\ & = \text{tr}(\Sigma_2) \text{tr}(\Sigma_4) \Sigma_1 \otimes \Sigma_3, \end{aligned}$$

here $\downarrow(\cdot)$ rearranges a matrix into a vector column by column and $\overrightarrow{(\cdot)}$ rearranges a matrix into a vector row by row. To notify the rank of Σ we have $\text{rank}(\Sigma) = \text{rank}(\Sigma_1) \text{rank}(\Sigma_3) =$



(a) An example of text-masked image.



(b) An example of palm-masked image.

Fig. 5. Comparisons of 2 scratched image recovery based on 7 algorithms.

$r_1 r_3$.

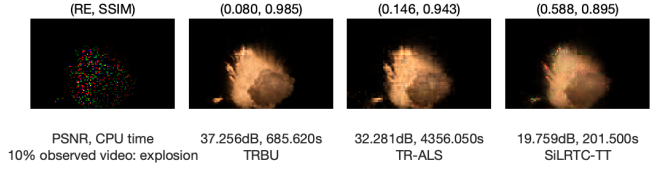
The next step is to verify the orthogonality (linear independence) of base, for which we use the modified version of the previous representation:

$$\sum_k w_{r_1 k}^{(1)} w_{k r_3}^{(2)} \sum_t w_{r_1 t}^{(1)} w_{t r_3}^{(2)} \sum_i u'_{ik} u''_{it} \sum_j v'_{jk} v''_{jt} \equiv 0,$$

where $\mathbf{U}' \neq \mathbf{U}''$ or $\mathbf{V}' \neq \mathbf{V}''$, which means the two pair of slices can not be the same at the same time, or it degenerates to the calculation of the squared ℓ_2 -norm. With this expression it is clear that both $\mathcal{U} = \mathcal{G}^{(1)} \overline{\otimes} \mathcal{G}^{(2)}$ and $\mathcal{V} = \mathcal{G}^{(3)} \overline{\otimes} \mathcal{G}^{(4)}$ are orthogonal.

Now we can be confident about the inferences that \mathcal{U} and \mathcal{V} are the (folded) singular tensors and Σ is the singular value matrix.

Generally there are $\mathbf{X}_{\{n,l\}} = \mathcal{U}_{(2)} \Sigma \mathcal{V}_{(2)}^T$ and $\text{rank}(\mathbf{X}_{\{n,l\}}) = r_n r_{n+l}$, where $\mathcal{U} = \overline{\otimes}_{k=n}^{n+l-1} \mathcal{G}^{(k)}$, $\mathcal{V} = \overline{\otimes}_{k=n+l}^{n-1} \mathcal{G}^{(k)}$ and $\Sigma = \prod_{k \neq n, n+l} \text{tr}(\Sigma_k) \Sigma_n \otimes \Sigma_{n+l}$, which shows the SVD of $\mathbf{X}_{\{n,l\}}$ is unique in the context of a (sub-)critical TR decomposition.



(a) An example of 10% observed video: explosion, the results are the last frame of the video.



(b) An example of 10% observed video: cock, the results are the first frame of the video.

Fig. 6. Comparisons of 2 scratched image recovery based on 7 algorithms.

APPENDIX B PROOF OF DEFINITION 1

Proof. Consider the core tensor $\mathcal{G}^{(k)}$, according to the identity $\sum_{i_k=1}^n H_{i_k}^2 = 1$, there is $E(H_{i_k}^2) = 1/n_k$, suppose that $H_{i_k} = \mathcal{G}_{t i_k s}^{(k)}$. Let $X_{ts} = \mathcal{G}_{t i_k s}^{(k)} \mathcal{G}_{t j_k s}^{(k)}$ and $S = \sum_t \sum_s X_{ts}$, obviously $E(S) = 0$ if $i_k \neq j_k$ and, if $i_k = j_k$ we have $E(S) = \sum_{t=1}^{r_k} \sum_{s=1}^{r_{k+1}} E(H_{i_k}^2) = r_k r_{k+1} / n_k$.

The proof to the assertion (Definition 1) is as follows. From the above deductions it is clear that $E(S) = \frac{r_k r_{k+1}}{n_k} \mathbf{1}_{i_k=j_k}$. Besides, according to the union bound $\max(\mathcal{G}^{(k)}) \leq \sqrt{\frac{\mu_{B_k}}{n}}$, the bound of X_{ts} is $C_1 = 2 \frac{\mu_{B_k}}{n_k}$. Incorporating Lemma 2 we have

$$P \left(|\langle \mathcal{G}_{i_k:}^{(k)}, \mathcal{G}_{j_k:}^{(k)} \rangle - \frac{r_k r_{k+1}}{n_k} \mathbf{1}_{i_k=j_k} | > \frac{\lambda \mu_{B_k} \sqrt{r_k r_{k+1}}}{n_k} \right) < 2e^{-\frac{\lambda^2}{2}},$$

let λ be a proportion of $\sqrt{\ln(n_k)}$, we prove (19) with

probability at least $1 - n_k^{-3}$ (say). Additionally, there is $\mu_k = O\left(\mu_{B_k} \sqrt{\ln(n_k)}\right)$.

Note that the above result is only for one core of TR, the total probability is $\prod_{k=1}^d (1 - n_k^{-3})$.

APPENDIX C

PROOF OF THEOREM 1

Proof. Suppose a d -order hypercubic tensor is considered, along with the TR-rank being r everywhere. Based on the assumption of Definition 1 and according to Lemma 1, there is no harm that we let all diagonal singular value matrices be \mathbf{E}_r except for arbitrary two. For convenience, assume that two singular value matrices are located at n and $n+l$, i.e., the locations of unfolding. To calculate the ℓ_2 -norm of the mode-2 fiber of $\overline{\otimes}_{k=n}^{n+l-1} \mathcal{G}^{(k)}$, recall that

$$\mathcal{X} = \sum_{s_1=1}^r \cdots \sum_{s_d=1}^r \mathcal{G}_{s_1:s_2}^{(1)} \circ \cdots \circ \mathcal{G}_{s_{d-1}:s_d}^{(d-1)} \circ \mathcal{G}_{s_d:s_1}^{(d)}.$$

First we pay attention to a simple case in which two core tensors have been contracted. By using MATLAB notation, the (r_1, r_3) -th mode-2 fiber of $\mathcal{G}^{(1)} \overline{\otimes} \mathcal{G}^{(2)}$ can be written as

$$\left(\mathcal{G}^{(1)} \overline{\otimes} \mathcal{G}^{(2)}\right)_{r_1:r_3} = \downarrow \left(\mathcal{G}_{r_1::}^{(1)} \mathcal{G}_{::r_3}^{(1)}\right),$$

the ℓ_2 -norm of the fiber is equal to the F-norm of the matrix which can be calculated by

$$\|\mathcal{G}_{r_1::}^{(1)} \mathcal{G}_{::r_3}^{(1)}\|_F = \|\mathbf{E}_r\|_F = r.$$

This equation is because mode-2 fibers of $\mathcal{G}^{(n)}$ are orthonormal. Let $\mathcal{G}^{(1)} \overline{\otimes} \mathcal{G}^{(2)}$ be a new core and we recursively repeat the above procedure, then the ℓ_2 -norm of the mode-2 fiber of $\overline{\otimes}_{k=n}^{n+l-1} \mathcal{G}^{(k)}$ is r^{p-1} .

Subsequently, we calculate the variable's expectation. Similar to the proof of Definition 1, let

$$\begin{aligned} H_{sit} &= \left(\overline{\otimes}_{k=n}^{n+l-1} \mathcal{G}^{(k)}\right)_{sit} \\ &= \left(\prod_{k=n}^{n+l-1} \mathcal{G}_{:i_k:}^{(k)}\right)_{st}, \end{aligned}$$

where $i \in \{1, \dots, 1 + \sum_{k=n}^{n+l-1} (i_k - 1) \prod_{m=n}^{k-1} i_m\}$. The result that $\mathbf{E}(H_{sit}^2) = r^{2p-2}/n^p$ can be easily derived from the truth that the ℓ_2 -norm of the mode-2 fiber is r^{p-1} . By letting

$$\begin{aligned} S &= \langle \mathcal{U}_{i::}, \mathcal{U}_{:j:} \rangle \\ &= \langle \left(\overline{\otimes}_{k=n}^{n+l-1} \mathcal{G}^{(k)}\right)_{i::}, \left(\overline{\otimes}_{k=n}^{n+l-1} \mathcal{G}^{(k)}\right)_{:j:} \rangle \\ &= \sum_s \sum_t H_{sit} H_{sjt}, \end{aligned}$$

we have $\mathbf{E}(S) = \frac{r^{2p}}{n^p} 1_{i=j}$, where the representation of j is the same with that of i above.

The variable's bound is determined by the following recurrence formula that stems from the assumption that only two cores are allowed to be contracted in each operation:

$$C_{k+1} = 2 \left(\sqrt{\frac{C_k}{2}} \sqrt{\frac{C_1}{2}} r \right)^2 = C_k \frac{\mu_B r^2}{n},$$

where $C_1 = 2 \frac{\mu_B}{n}$. The closed-form of the above equation is

$$C_k = C_1 \left(\frac{\mu_B r^2}{n} \right)^{k-1},$$

$$\text{thus } C_p = 2 \left(\frac{\mu_B}{n} \right)^p r^{2p-2}.$$

Notice that the singular vectors are not normalized, we normalize them by dividing the ℓ_2 -norm r^{p-1} , thus the singular tensors become

$$\begin{cases} \mathcal{U} = \frac{1}{r^{p-1}} \overline{\otimes}_{k=n}^{n+l-1} \mathcal{G}^{(k)} \\ \mathcal{V} = \frac{1}{r^{q-1}} \overline{\otimes}_{k=n+l}^{n+l-1} \mathcal{G}^{(k)} \end{cases}$$

and there are $\mathbf{E}(S) = \frac{r^2}{n^p} 1_{i=j}$ and $C_p = 2 \frac{\mu_B^p}{n^p}$. It is trivial to verify that $C_p < C_1$ for enough large n . By Lemma 2, we have

$$\mathbf{P} \left(|\langle \mathcal{U}_{i::}, \mathcal{U}_{:j:} \rangle - \frac{r^2}{n^p} 1_{i=j}| > t \right) < 2e^{-\frac{2t^2}{r^2 C_p^2}},$$

the right term can be simplified to $2e^{-\frac{2t^2}{r^2 C_p^2}} = 2e^{-\frac{t^2}{2r^2 \mu_B^2 / n^{2p}}}$. Let $t = \frac{\lambda \mu_B^p r}{n^p}$, the right term becomes $2e^{-\frac{\lambda^2}{2}}$. Choosing $\lambda = O(\sqrt{p \ln(n)})$, inequality

$$|\langle \mathcal{U}_{i::}, \mathcal{U}_{:j:} \rangle - \frac{r^2}{n^p} 1_{i=j}| \leq \frac{\lambda \mu_B^p r}{n^p}$$

holds with probability at least $1 - n^{-3p}$, and the parameter $\mu'_{1k} = \lambda \mu_B^p$ is derived.

The proof of

$$|\langle \mathcal{V}_{i::}, \mathcal{V}_{:j:} \rangle - \frac{r^2}{n^q} 1_{i=j}| \leq \frac{\mu'_{2k} r}{n^q}$$

is the same as \mathcal{U} 's by taking $\lambda = O(\sqrt{q \ln(n)})$ and $\mu'_{2k} = \lambda \mu_B^q$, which holds with probability at least $1 - n^{-3q}$.

Besides, let $X_{st} = \left(\overline{\otimes}_{k=n}^{n+l-1} \mathcal{G}^{(k)}\right)_{sit} \left(\overline{\otimes}_{k=n+l}^{n+l-1} \mathcal{G}^{(k)}\right)_{st}$, it is evident that $\mathbf{E}(X_{st}) \equiv 0$, and the variable's bound satisfies $C_{pq} = \frac{r^{2p-2}}{n^p} \cdot \frac{r^{2q-2}}{n^q} = \frac{r^{2d-4}}{n^d}$. Normalizing \mathcal{U} and \mathcal{V} by dividing r^{p-1} and r^{q-1} respectively, we have $C_{pq} = 2 \left(\frac{\mu_B}{n} \right)^d$ and

$$\mathbf{P} (|\langle \mathcal{U}_{i::}, \mathcal{V}_{:j:} \rangle| > t) < 2e^{-\frac{2t^2}{r^2 C_{pq}^2}},$$

by choosing $t = \frac{\mu_B^d r}{\sqrt{n^d}}$, the following inequality

$$|\langle \mathcal{U}_{i::}, \mathcal{V}_{:j:} \rangle| \leq \frac{\mu_B^d r}{\sqrt{n^d}}$$

holds with probability at least $1 - e^{-n^{d/2}}$, and $\mu'' = \mu_B^d$.

For a “sign” TR, i.e., $\Sigma_1 = \mathbf{E}_{r_1}, \dots, \Sigma_d = \mathbf{E}_{r_d}$, the ℓ_2 -norm of the fibers of \mathcal{U} and \mathcal{V} are $\prod_{k=n}^{n+l-1} r_k$ and $\prod_{k=n+l+1}^{n+l-1} r_k$ respectively and hence $\mathbf{E}(S) = \frac{r_n r_{n+l}}{\prod_{k=n}^{n+l-1} r_k} 1_{i=j}$, $C_p = 2 \prod_{k=n}^{n+l-1} \frac{\mu_{B_k}}{n_k}$ and $C_{pq} = 2 \prod_{k=1}^d \frac{\mu_{B_k}}{n_k}$. Additionally,

the orthonormal singular tensors are

$$\begin{cases} \mathcal{U} = \prod_{k=n+1}^{n+l-1} \frac{1}{r_k} \otimes_{k=n}^{n+l-1} \mathcal{G}^{(k)} \\ \mathcal{V} = \prod_{k=n+l+1}^{n-1} \frac{1}{r_k} \otimes_{k=n+l}^{n-1} \mathcal{G}^{(k)} \end{cases},$$

Accordingly, the following inequalities holds with high probabilities:

$$\begin{cases} |\langle \mathcal{U}_{:i}, \mathcal{U}_{:j} \rangle - \frac{r_n r_{n+l}}{\prod_{k=n}^{n+l-1} n_k} \mathbf{1}_{i=j}| \leq \frac{\mu'_{1nl} \sqrt{r_n r_{n+l}}}{\prod_{k=n}^{n+l-1} n_k} \\ |\langle \mathcal{V}_{:i}, \mathcal{V}_{:j} \rangle - \frac{r_n r_{n+l}}{\prod_{k=n+l+1}^{n-1} n_k} \mathbf{1}_{i=j}| \leq \frac{\mu'_{2nl} \sqrt{r_n r_{n+l}}}{\prod_{k=n+l+1}^{n-1} n_k} \end{cases}$$

holds with probabilities at least $1 - \prod_{k=n}^{n+l-1} n_k^{-3}$ and $1 - \prod_{k=n+l+1}^{n-1} n_k^{-3}$ respectively and

$$|\langle \mathcal{U}_{:i}, \mathcal{V}_{:j} \rangle| \leq \frac{\mu'' \sqrt{r_n r_{n+l}}}{\sqrt{\prod_{k=1}^d n_k}},$$

holds with probabilities at least $1 - e^{-\frac{1}{2} \prod_{k=1}^d n_k}$, where

$$\begin{cases} \mu'_{1nl} = O \left(\prod_{k=n}^{n+l-1} \mu_{B_k} \sqrt{\sum_{k=n}^{n+l-1} \ln n_k} \right) \\ \mu'_{2nl} = O \left(\prod_{k=n+l+1}^{n-1} \mu_{B_k} \sqrt{\sum_{k=n+l+1}^{n-1} \ln n_k} \right) \\ \mu'' = \prod_{k=1}^d \mu_{B_k} \end{cases}.$$

Here we accomplish the proof of Theorem 1.

APPENDIX D PROOF OF THEOREM 2

Proof. Recall that the dual certificate for the nuclear norm minimization of $\mathbf{X}_{\{n,l\}}$ is that there exists $\mathcal{Y} \in \mathbb{R}^{n_1 \times \dots \times n_d}$ obeying

$$\begin{cases} \mathcal{P}_\Omega(\mathcal{Y}) = \mathcal{Y} \\ \mathcal{P}_{T_{nl}}(\mathcal{Y}) = \prod_{k \neq n, n+l} \frac{1}{r_k} \mathcal{R}, \\ \|\mathcal{P}_{T_{nl}^\perp}(\mathcal{Y})\|_2 < 1 \end{cases}$$

where \mathcal{P} means the projection, T_{nl} is the spanned space defined as

$$T_{nl} = \{ \mathbf{T} | \mathbf{T} = \prod_{k=n+1}^{n+l-1} \frac{1}{r_k} \mathcal{U}_{(2)} \mathbf{Y}^T + \prod_{k=n+l+1}^{n-1} \frac{1}{r_k} \mathbf{X} \mathcal{V}_{(2)}^T, \\ \forall \mathbf{X}, \mathbf{Y} \in \mathbb{R}^{\prod_{k=n}^{n+l-1} n_k \times \prod_{k=n+l+1}^{n-1} n_k} \}$$

and \mathcal{R} is the companion tensor generated by the TR in which all singular value matrices are identity matrices.

The prove of this dual certificate is skipped. It is easy to be proved based on the truth of Theorem 1, as [41] declares the result in Lemma 3 is general and nonasymptotic. Then

solving (30) gives the exact solution \mathcal{X} with probability at least $1 - n_l^{-3}$

APPENDIX E PROOF OF LEMMA 4

Proof. We first prove the comparable condition. If the elements in a vector \mathbf{x} are comparable, from the geometrical viewpoint the vector \mathbf{x} must be closed to another vector $\mathbf{v} = [k, \dots, k]^T$, where $k = \mathbf{x}^T \mathbf{e}$ is the projection of vector \mathbf{x} on unit vector $\mathbf{e} = [1, \dots, 1]^T / \sqrt{N}$. It means that the included angle between \mathbf{x} and \mathbf{v} is very small, i.e., $\cos \theta = \|\mathbf{v}\|_2 / \|\mathbf{x}\|_2 = 1 - \epsilon'$, where ϵ' is a small positive number. Hence we have $\|\mathbf{x}\|_1 = (1 - \epsilon') \sqrt{N} \|\mathbf{x}\|_2$, which means $|\|\mathbf{x}\|_1 - \sqrt{N} \|\mathbf{x}\|_2| = \epsilon' \sqrt{N} \|\mathbf{x}\|_2 \leq \epsilon$.

Suppose $\|\mathbf{x}\|_1 = \sqrt{N} \|\mathbf{x}\|_2$, i.e., $x_1 = x_2 = \dots = x_N$. It is clear that $\alpha + \beta$ is minimal when $\delta = 0$, as the mean value inequality $\sqrt{\prod_{i=1}^N x_i} = \sqrt{\alpha \beta} \leq (\alpha + \beta) / 2$ reveals that the objective function $\alpha + \beta$ becomes smaller when α and β getting closer. As for $\|\mathbf{x}\|_1 \neq \sqrt{N} \|\mathbf{x}\|_2$, we examine sequence $\{\beta/\alpha\}$ which monotonically decreases from a ($a > 1$) to b ($b < 1$) with increasing n . Therefore, appropriate δ and ξ must exist such that when $n = \lceil N/2 \rceil + \delta$,

$$a \geq \left(\frac{\beta}{\alpha} \right)_{n-1} > \left(\frac{\beta}{\alpha} \right)_n = 1 + \xi > \left(\frac{\beta}{\alpha} \right)_{n+1} \geq b.$$

In this way, the objective function $|\beta/\alpha - 1|$ gets its minimum.

The proof is complete.

REFERENCES

- [1] T. G. Kolda and B. W. Bader, "Tensor decompositions and applications," *SIAM Review*, vol. 51, no. 3, pp. 455–500, 2009.
- [2] A. Cichocki, D. Mandic, L. De Lathauwer, G. Zhou, Q. Zhao, C. Caiafa, and H. A. Phan, "Tensor decompositions for signal processing applications: from two-way to multiway component analysis," *IEEE Signal Processing Magazine*, vol. 32, no. 2, pp. 145–163, 2015.
- [3] A. Cichocki, N. Lee, I. Oseledets, A.-H. Phan, Q. Zhao, D. P. Mandic, et al., "Tensor networks for dimensionality reduction and large-scale optimization: part 1 low-rank tensor decompositions," *Foundations and Trends® in Machine Learning*, vol. 9, no. 4-5, pp. 249–429, 2016.
- [4] S. Gandy, B. Recht, and I. Yamada, "Tensor completion and low-n-rank tensor recovery via convex optimization," *Inverse Problems*, vol. 27, no. 2, p. 025010, 2011.
- [5] N. D. Sidiropoulos, L. De Lathauwer, X. Fu, K. Huang, E. E. Papalexakis, and C. Faloutsos, "Tensor decomposition for signal processing and machine learning," *IEEE Transactions on Signal Processing*, vol. 65, no. 13, pp. 3551–3582, 2017.
- [6] M. Signoretto, R. Van de Plas, B. De Moor, and J. A. Suykens, "Tensor versus matrix completion: a comparison with application to spectral data," *IEEE Signal Processing Letters*, vol. 18, no. 7, pp. 403–406, 2011.
- [7] J. Liu, P. Musialski, P. Wonka, and J. Ye, "Tensor completion for estimating missing values in visual data," *IEEE Transactions on Pattern Analysis and Machine Intelligence*, vol. 35, no. 1, pp. 208–220, 2013.
- [8] M. Lubasch, J. I. Cirac, and M.-C. Banuls, "Algorithms for finite projected entangled pair states," *Physical Review B*, vol. 90, no. 6, p. 064425, 2014.
- [9] Z. Long, Y. Liu, L. Chen, and C. Zhu, "Low rank tensor completion for multiway visual data," *Signal Processing*, 2018.
- [10] C. J. Hillar and L.-H. Lim, "Most tensor problems are NP-hard," *Journal of the ACM*, vol. 60, no. 6, p. 45, 2013.
- [11] Y. Liu, F. Shang, L. Jiao, J. Cheng, and H. Cheng, "Trace norm regularized CANDECOMP/PARAFAC decomposition with missing data," *IEEE Transactions on Cybernetics*, vol. 45, no. 11, pp. 2437–2448, 2015.
- [12] Y. Liu, F. Shang, W. Fan, J. Cheng, and H. Cheng, "Generalized higher order orthogonal iteration for tensor learning and decomposition," *IEEE Transactions on Neural Networks and Learning Systems*, vol. 27, no. 12, pp. 2551–2563, 2016.

- [13] L. Yang, J. Fang, H. Li, and B. Zeng, "An iterative reweighted method for Tucker decomposition of incomplete tensors," *IEEE Transactions on Signal Processing*, vol. 64, no. 18, pp. 4817–4829, 2016.
- [14] J. A. Bazerque, G. Mateos, and G. B. Giannakis, "Rank regularization and Bayesian inference for tensor completion and extrapolation," *IEEE transactions on signal processing*, vol. 61, no. 22, pp. 5689–5703, 2013.
- [15] Y. Xu and W. Yin, "A block coordinate descent method for regularized multiconvex optimization with applications to nonnegative tensor factorization and completion," *SIAM Journal on Imaging Sciences*, vol. 6, no. 3, pp. 1758–1789, 2013.
- [16] Q. Zhao, L. Zhang, and A. Cichocki, "Bayesian CP factorization of incomplete tensors with automatic rank determination," *IEEE Transactions on Pattern Analysis and Machine Intelligence*, vol. 37, no. 9, pp. 1751–1763, 2015.
- [17] Y. Yang, Y. Feng, and J. A. Suykens, "A rank-one tensor updating algorithm for tensor completion," *IEEE Signal Processing Letters*, vol. 22, no. 10, pp. 1633–1637, 2015.
- [18] Y. Yang, Y. Feng, X. Huang, and J. A. Suykens, "Rank-1 tensor properties with applications to a class of tensor optimization problems," *SIAM Journal on Optimization*, vol. 26, no. 1, pp. 171–196, 2016.
- [19] T. Yokota, Q. Zhao, and A. Cichocki, "Smooth PARAFAC decomposition for tensor completion," *IEEE Transactions on Signal Processing*, vol. 64, no. 20, pp. 5423–5436, 2016.
- [20] Y. Liu and F. Shang, "An efficient matrix factorization method for tensor completion," *IEEE Signal Processing Letters*, vol. 20, no. 4, pp. 307–310, 2013.
- [21] L. Yang, Z.-H. Huang, and X. Shi, "A fixed point iterative method for low n -rank tensor pursuit," *IEEE Transactions on Signal Processing*, vol. 61, no. 11, pp. 2952–2962, 2013.
- [22] M. K.-P. Ng, Q. Yuan, L. Yan, and J. Sun, "An adaptive weighted tensor completion method for the recovery of remote sensing images with missing data," *IEEE Transactions on Geoscience and Remote Sensing*, vol. 55, no. 6, pp. 3367–3381, 2017.
- [23] B. Romera-Paredes and M. Pontil, "A new convex relaxation for tensor completion," in *Advances in Neural Information Processing Systems*, pp. 2967–2975, 2013.
- [24] D. Kressner, M. Steinlechner, and B. Vandeheycken, "Low-rank tensor completion by Riemannian optimization," *BIT Numerical Mathematics*, vol. 54, no. 2, pp. 447–468, 2014.
- [25] C. Mu, B. Huang, J. Wright, and D. Goldfarb, "Square deal: Lower bounds and improved relaxations for tensor recovery," in *International Conference on Machine Learning*, pp. 73–81, 2014.
- [26] Y. Xu, R. Hao, W. Yin, and Z. Su, "Parallel matrix factorization for low-rank tensor completion," *Inverse Problems and Imaging*, vol. 9, no. 2, pp. 601–624, 2015.
- [27] M. E. Kilmer, K. Braman, N. Hao, and R. C. Hoover, "Third-order tensors as operators on matrices: a theoretical and computational framework with applications in imaging," *SIAM Journal on Matrix Analysis and Applications*, vol. 34, no. 1, pp. 148–172, 2013.
- [28] Z. Zhang and S. Aeron, "Exact tensor completion using t-SVD," *IEEE Transactions on Signal Processing*, vol. 65, no. 6, pp. 1511–1526, 2017.
- [29] Z. Zhang, G. Ely, S. Aeron, N. Hao, and M. Kilmer, "Novel methods for multilinear data completion and de-noising based on tensor-SVD," in *Proceedings of the IEEE Conference on Computer Vision and Pattern Recognition*, pp. 3842–3849, 2014.
- [30] X.-Y. Liu, S. Aeron, V. Aggarwal, X. Wang, and M.-Y. Wu, "Tensor completion via adaptive sampling of tensor fibers: application to efficient indoor RF fingerprinting," in *Acoustics, Speech and Signal Processing (ICASSP), 2016 IEEE International Conference on*, pp. 2529–2533, IEEE, 2016.
- [31] I. V. Oseledets, "Tensor-train decomposition," *SIAM Journal on Scientific Computing*, vol. 33, no. 5, pp. 2295–2317, 2011.
- [32] W. Wang, V. Aggarwal, and S. Aeron, "Tensor completion by alternating minimization under the tensor train (TT) model," *arXiv preprint arXiv:1609.05587*, 2016.
- [33] L. Yuan, Q. Zhao, and J. Cao, "Completion of high order tensor data with missing entries via tensor-train decomposition," in *International Conference on Neural Information Processing*, pp. 222–229, Springer, 2017.
- [34] J. A. Benua, H. N. Phien, H. D. Tuan, and M. N. Do, "Efficient tensor completion for color image and video recovery: low-rank tensor train," *IEEE Transactions on Image Processing*, vol. 26, no. 5, pp. 2466–2479, 2017.
- [35] L. Grasedyck, M. Kluge, and S. Krämer, "Variants of alternating least squares tensor completion in the tensor train format," *SIAM Journal on Scientific Computing*, vol. 37, no. 5, pp. A2424–A2450, 2015.
- [36] W. Wang, V. Aggarwal, and S. Aeron, "Efficient low rank tensor ring completion," in *Computer Vision (ICCV), 2017 IEEE International Conference on*, IEEE, 2017.
- [37] Y. Liu, Z. Long, and C. Zhu, "Image completion using low tensor tree rank and total variation minimization," *IEEE Transactions on Multimedia*, pp. 1–1, 2018.
- [38] Q. Zhao, M. Sugiyama, and A. Cichocki, "Learning efficient tensor representations with ring structure networks," *arXiv preprint arXiv:1705.08286*, 2017.
- [39] K. Ye and L.-H. Lim, "Tensor network ranks," *arXiv preprint arXiv:1801.02662*, 2018.
- [40] M. Fazel, *Matrix rank minimization with applications*. PhD thesis, PhD thesis, Stanford University, 2002.
- [41] E. J. Candès and T. Tao, "The power of convex relaxation: Near-optimal matrix completion," *IEEE Transactions on Information Theory*, vol. 56, no. 5, pp. 2053–2080, 2010.
- [42] L. Warnke, "On the method of typical bounded differences," *Combinatorics, Probability and Computing*, vol. 25, no. 2, pp. 269–299, 2016.
- [43] I. V. Oseledets and E. E. Tyrtyshnikov, "Tensor tree decomposition does not need a tree," *preprint*, vol. 8, 2009.
- [44] S. Ma, D. Goldfarb, and L. Chen, "Fixed point and Bregman iterative methods for matrix rank minimization," *Mathematical Programming*, vol. 128, no. 1-2, pp. 321–353, 2011.
- [45] R. Nishihara, L. Lessard, B. Recht, A. Packard, and M. I. Jordan, "A general analysis of the convergence of admm," *arXiv preprint arXiv:1502.02009*, 2015.
- [46] Z. Lin, M. Chen, and Y. Ma, "The augmented lagrange multiplier method for exact recovery of corrupted low-rank matrices," *arXiv preprint arXiv:1009.5055*, 2010.
- [47] C. Lu, *A Library of ADMM for Sparse and Low-rank Optimization*. National University of Singapore, June 2016. <https://github.com/canyilu/LibADMM>.
- [48] M. F. Barnsley and L. P. Hurd, *Fractal image compression*, vol. 1. AK Peters Wellesley, 1993.
- [49] Z. Wang, E. Simoncelli, A. Bovik, *et al.*, "Multi-scale structural similarity for image quality assessment," in *ASILOMAR Conference on Signals Systems and Computers*, vol. 2, pp. 1398–1402, IEEE, 1998, 2003.
- [50] J. I. Latorre, "Image compression and entanglement," *arXiv preprint quant-ph/0510031*, 2005.